Tunneling Dynamics in Multiphoton Ionization and Attoclock Calibration

Michael Klaiber, Karen Z. Hatsagortsyan,* and Christoph H. Keitel
Max-Planck-Institut für Kernphysik, Saupfercheckweg 1, 69117 Heidelberg, Germany
(Received 29 July 2014; published 23 February 2015; corrected 29 July 2015)

The intermediate domain of strong-field ionization between the tunneling and multiphoton regimes is investigated using the strong-field approximation and the imaginary-time method. An intuitive model for the dynamics is developed which describes the ionization process within a nonadiabatic tunneling picture with a coordinate dependent electron energy during the under-the-barrier motion. The nonadiabatic effects in the elliptically polarized laser field induce a transversal momentum shift of the tunneled electron wave packet at the tunnel exit and a delayed appearance in the continuum as well as a shift of the tunneling exit towards the ionic core. The latter significantly modifies the Coulomb focusing during the electron excursion in the laser field after exiting the ionization tunnel. We show that nonadiabatic effects are especially large when the Coulomb field of the ionic core is taken into account during the under-the-barrier motion. The simple man model modified with these nonadiabatic corrections provides an intuitive background for exact theories and has direct implications for the calibration of the attoclock technique.

DOI: 10.1103/PhysRevLett.114.083001 PACS numbers: 32.80.Rm, 03.65.Xp

In intense near-infrared laser fields, when the photon energy is much less than the ionization energy of the atomic system, the atomic ionization happens via multiphoton processes [1,2]. The multiphoton and tunneling regimes have been identified as well-known asymptotic limits [3], with the latter following an especially intuitive tunneling picture. In this case the laser field is so strong that the bound electron tunnels with a constant energy through the (quasi)static potential barrier formed by the laser field and the atomic potential (the horizontal channel in phase space at a constant energy of the ionizing electron [4–6]; see Fig. 1). The quasistatic (adiabatic) dynamics is characterized by an asymptotically small Keldysh parameter $\gamma \ll 1$, where $\gamma = \kappa\omega/E_0$, $I_p = \kappa^2/2$ is the ionization potential, E_0 the laser electric field strength, and ω the laser angular frequency. In the opposite asymptotic limit $\gamma \gg 1$ of the multiphoton regime, the electron release from the bound state happens at the atomic core via overcoming the atomic potential due to the absorption of multiple laser photons by the bound electron (the vertical channel in phase space at a constant coordinate of the ionizing electron [5,6]; see Fig. 1). The strong-field ionization in both regimes can be described analytically in the strong-field approximation [3,7,8] and via the imaginary time method [9–13], which is also applied for arbitrary Keldysh parameters [14–18]. It is straightforward to deduce from the quasistatic theory the parameters of the tunneling picture, such as the coordinate of the tunnel exit and the electron momentum at the tunnel exit [19]. However, it is not clear how the intuitive picture is gradually transformed from the horizontal tunneling [4] to the vertical multiphoton channel within the intermediate regime. While the intuitive picture is appealing *per se*, it also allows us to predict how the tunneling exit coordinate and the electron momentum at the exit are qualitatively modified in the nonadiabatic domain. The latter is important because these parameters are required for the attoclock calibration [19–22]. In the attoclock [20] the time of the electron's appearance in the continuum is mapped onto the angle of the photoelectron emission. For its calibration the emission angle should be corrected by the amount originating from Coulomb focusing which is determined by the tunneling parameters.

Recent experimental investigations of nonadiabatic effects for the attoclock calibration indicated no significant impact of these effects on the distribution of the photoelectron momentum up to a Keldysh parameter of $\gamma \approx 3.8$ [6], and the difference between the quasistatic calculations and the experimental results was attributed to a tunneling delay time. However, numerical simulations [23] and an R-matrix theory calculation [24,25] concluded that the observed photoelectron emission momentum distribution is explained by a vanishing tunneling time delay when the Coulomb field of the atomic core is taken fully into account [26].

In this Letter we put forward an intuitive picture for the intermediate regime of ionization, describing it as tunneling through a classically forbidden region with a coordinate dependent rising energy due to the time-dependent barrier. The picture allows us to deduce in a simple way the characteristics of the under-the-barrier motion and shows how the semiclassical theory of Ref. [6] should be remedied to describe the observed photoelectron spectra, explaining the discrepancy between results of Refs. [6] and [26]. Nonadiabatic effects induce a transversal momentum shift of the electron at the tunneling exit and a delayed appearance in the continuum as well as a shift of the tunneling exit coordinate towards the ionic core. While for the asymptotic momentum distribution in the case of a

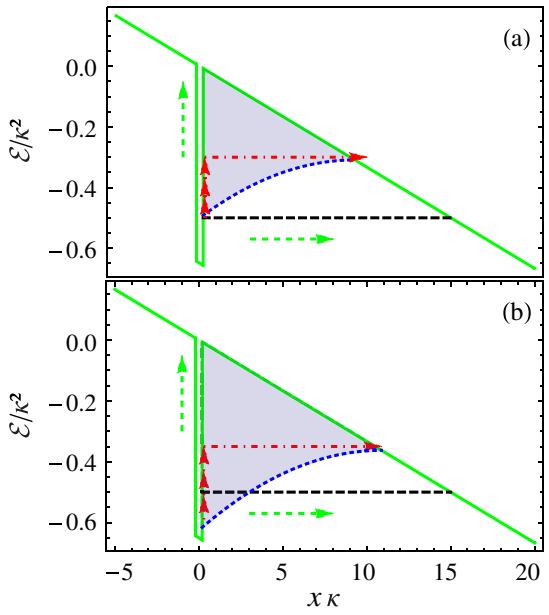

FIG. 1 (color online). The tunneling barrier of ionization in the case of a short-range atomic potential (solid, green line). The electron energy during the under-the-barrier motion: the nonadiabatic (short-dashed, blue line) and adiabatic (quasistatic) pictures (long-dashed, black line) in a (a) linearly or (b) circularly polarized laser field. The horizontal channel (tunneling) and the vertical channel (multiphoton ionization) are shown schematically by dashed green arrows. The interpretation of nonadiabatic tunneling as absorption of photons followed by tunneling with higher energy is shown with the (dot-dashed, red arrows) pathway in (a).

short-range atomic potential all three effects almost compensate for each other, the effect of the shift of the tunneling exit dominates when the Coulomb field of the atomic core is accurately taken into account in the under-the-barrier motion. This has a decisive impact on the Coulomb focusing during the motion in the continuum after tunneling and, consequently, on the final momentum distribution and on attoclock calibration.

For the analysis we employ the strong-field approximation (SFA) with the saddle point approximation including nonadiabatic corrections and quantify the effect of nonadiabatic corrections on the attoclock calibration. For the sake of simplicity let us begin with modeling the atomic system with a three-dimensional short-range potential V_s. The ionization dynamics is described by the Hamiltonian

$$H = \hat{\mathbf{p}}^2/2 + V_s(\mathbf{r}) + \mathbf{r}\cdot\mathbf{E}(t), \tag{1}$$

where $\hat{\mathbf{p}}$ is the momentum operator, $\mathbf{E}(t) = -E_0(\cos\omega t, \epsilon\sin\omega t)$ the laser field of elliptical polarization with laser ellipticity ϵ (atomic units are used throughout the Letter). According to SFA the ionized wave packet in momentum space at some time t, when the laser pulse is turned off, reads [2]

$$\psi(\mathbf{p},t) = \int_{-\infty}^{t} dt' \langle \mathbf{p} + \mathbf{A}(t')|V_s|\phi_b\rangle \times \exp[-iS_L(t,t',\mathbf{p}) + iI_p t'], \tag{2}$$

with the constant matrix element of the short-range potential $\langle \mathbf{p} + \mathbf{A}(t')|V_s|\phi_b\rangle$ and the bound state $|\phi_b\rangle$. $S_L(t,t',\mathbf{p}) = \int_{t'}^{t} d\tilde{t}\,\mathcal{E}(\tilde{t},\mathbf{p})$ is the classical action of the active electron in the laser field, $\mathcal{E}(t,\mathbf{p}) \equiv \mathbf{p}(t)^2/2 = (\mathbf{p} + \mathbf{A}(t))^2/2$ the energy of the electron in the laser field with the asymptotic electron momentum $\mathbf{p}$ and the laser vector potential $\mathbf{A}(t)$, $\mathbf{E}(t) = -\partial_t\mathbf{A}(t)$. We assume that the photon energy of the laser field is much smaller than the ionization (I_p) and ponderomotive ($U_p = E_0^2/2\omega^2$) energies $\omega \ll I_p, U_p$. Then the integral in Eq. (2) can be solved via the saddle point method (SPM), which defines the initial time of ionization $t' = t_s$ via $\mathcal{E}(t_s,\mathbf{p}) = -\kappa^2/2$, describing the energy conservation when the electron starts to leave the bound state. This, here called saddle time, t_s, is complex due to the negative binding energy $-\kappa^2/2$. The motion of the electron can be described by two steps. The first step is a motion in the classically forbidden region where the time runs from the initial complex saddle time to the real time axis. When the time reaches the real axis at t_e, representing the tunnel exit time, the free motion in the laser field begins and from that time on runs along the real axis. The ionization probability does not change after $t > t_e$ and, therefore, is determined by the exponent

$$\Gamma \sim |\psi(\mathbf{p},t)|^2 \sim \exp[-2iS_L(t_e,t_s,\mathbf{p}) + 2iI_p t_s], \tag{3}$$

which is a function of the final momentum $\mathbf{p}$ or, equivalently, of the tunneling phase [14]. Thus, in the physical situation suitable for the SPM ($\omega \ll I_p, U_p$), at any value of the Keldysh parameter, during the ionization the electron penetrates the classically forbidden region. This dynamics can be termed tunneling, although at large γ the energy is not conserved during the tunneling, as we will show below.

We generalize the quasistatic picture of tunneling into the nonadiabatic regime as follows. While in the quasistatic case the electron energy is constant during tunneling, in the nonadiabatic regime the electron gains energy in the course of the under-the-barrier motion. In the quasistatic case [see Fig. 1 (ionization at the peak of the laser field is considered, $t_e = 0$, $p_x = 0$)], the electron tunnels through the effective potential $V_{\text{eff}}(x) = V_s - xE_0$ (which can be defined in a gauge-invariant manner—see Ref. [27]; solid green line) on a constant energy level (long-dashed black line) $\mathcal{E} = -I_p$, where $\mathcal{E} = \mathcal{E}_\parallel + V_{\text{eff}}$ is the total energy, with the kinetic energy along the tunneling direction $\mathcal{E}_\parallel = p_x(t)^2/2 = A(t)^2/2 = E_0^2 t^2/2$ (negative during the under-the-barrier motion). In the nonadiabatic case the electron energy is not constant during the motion in the classically forbidden region and depends on the coordinate along the tunneling direction:

$$\mathcal{E}(x) = \mathcal{E}_{\parallel}(x) + V_{\text{eff}}(x), \tag{4}$$

which can be derived accurately by calculating the electron kinetic energy in the laser field $\mathcal{E}_{\parallel}(t) = A_x(t)^2/2 = [(E_0/\omega)\sin(\omega t)]^2/2$ and taking into account the electron trajectory under the barrier $x(t) = \int_{t_s}^{t} dt' A_x(t')$. As the short-dashed blue lines in Fig. 1 shows, the electron energy increases during tunneling, which induces the shift of the tunneling exit towards the atomic core. In a linearly polarized laser field the coordinate dependence of the energy level can be calculated analytically (see Ref. [28]): $\mathcal{E}(x) = \kappa^2[1 - (\sqrt{\gamma^2+1} - \gamma\kappa x/2n)^2]/2\gamma^2 - xE_0$, with $n = I_p/\omega$. In this way one can represent the strong-field ionization in the low-frequency regime ($\omega \ll I_p, U_p$) as tunneling with a coordinate dependent energy, which is due to the electron energy gain from the varying barrier. We have estimated the shift of the exit coordinate towards the atomic core due to nonadiabatic effects via $x_e = \int_{t_s}^{t_e} dt A_x(t) = x_{e,qs} - \delta x$, with the exit coordinate in the quasistatic case $x_{e,qs} = \kappa^2/2E_0$ and the nonadiabatic correction $\delta x = (1 - (4\epsilon^2/9))(\gamma^2/4)x_{e,qs}$; see Ref. [28]. As Fig. 2(b) shows, the coordinate of the electron's appearance in the continuum in the nonadiabatic regime is smaller in comparison to the quasistatic case, however, it increases with larger γ.

The intuitive picture of Fig. 1 not only indicates the change of the tunneling exit due to nonadiabatic effects but can also hint at how the ionization probability is modified. The tunneling probability in Eq. (3) can be represented for $\gamma \lesssim 1$ as follows (for a linearly polarized field) [28]:

$$\Gamma \sim \exp\left[2i\left(\int_{x_i}^{x_e} p_x(t(x))dx - \int_{t_s}^{t_e}\left[\frac{p_x(t)^2}{2} - xE(t)\right]dt + I_p t_s\right)\right], \tag{5}$$

where $E(t) = -\mathbf{e}_x \cdot \mathbf{E}(t)$. In the static, pure tunneling case the last two terms of the equation cancel due to energy conservation, whereas in the pure multiphoton regime of large γ, the last term dominates and gives the well-known $\Gamma \sim \mathcal{I}^n$ rule, with the laser intensity $\mathcal{I}$ and $n = I_p/\omega$. In the intermediate regime that is considered here, all three terms contribute. For $\gamma \lesssim 1$, a modified tunneling exponent can be derived [28],

$$\Gamma \sim \exp\left[2i(1+\gamma^2/5)\int_{x_i}^{x_e} p_x(t(x))dx\right] \tag{6}$$

where the leading order correction due to the last two terms of Eq. (5) is included. As the exponent in Eq. (6) is proportional to $\int_{x_i}^{x_e} p_x(t(x))dx$, the ionization in the intermediate regime $\gamma \lesssim 1$ can again be called tunneling.

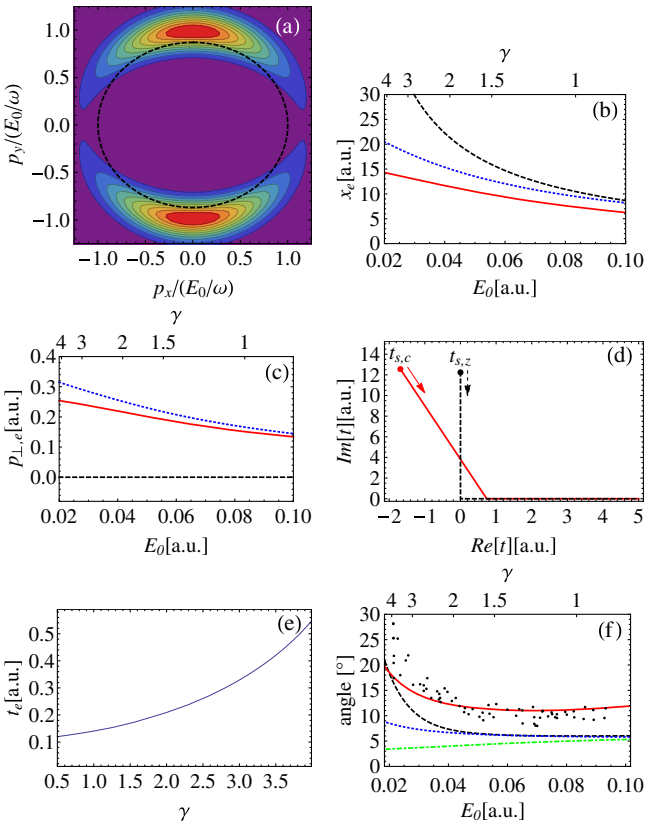

FIG. 2 (color online). Ionization in a laser field with ellipticity of $\epsilon = 0.87$. (a) The asymptotic momentum distribution and the corresponding quasistatic result are shown as a dashed ellipse for $\gamma = 1$. (b) The exit coordinate vs the Keldysh parameter. (c) The most probable transverse momentum at the tunneling exit $p_{\perp e}$ vs the Keldysh parameter. (d) The complex time contour during tunneling in the Coulomb potential (the red, solid line) and the zero-range potential (black, dashed line) for $E_0 = 0.1$ a.u. (the arrows show the integration direction). (e) The nonadiabatic time delay t_e vs the Keldysh parameter at $E_0 = 0.02$ a.u. (f) The emission angle of the most probable photoelectrons vs the Keldysh parameter. In (b), (c), and (f) the nonadiabatic case for the Coulomb potential (the red, solid line), the quasistatic case in the Coulomb potential (the black, long-dashed line), and the nonadiabatic case in the zero-range potential (the blue, short-dashed line) are plotted. In (f) only the nonadiabatic momentum shift at the tunnel exit (the green, dot-dashed line) is taken into account in the otherwise quasistatic case of a zero-range potential, and experimental data of Ref. [6] are displayed as black dots.

The area between the potential barrier and the energy level in Fig. 1 can qualitatively indicate the ionization probability. Moreover, one can give a rule of thumb for the ionization rate in the $\gamma \lesssim 1$ region, describing it as $\tilde{n}$-photon absorption followed by static tunneling at higher energy $\mathcal{E} = -I_p + \tilde{n}\omega$ [see the red path in Fig. 1]:

$$\Gamma \sim \mathcal{I}^{\tilde{n}} \exp\left[-\int_{x_i}^{x_e} p_{qs}(x)dx\right], \tag{7}$$

with effective photon number $\tilde{n} = \delta\mathcal{E}/\omega$, energy change during the under-the-barrier motion $\delta\mathcal{E} = (x_{e,qs} - x_e)E_0$, and $p_{qs}(x) = \sqrt{-xE_0 - (-I_p + \tilde{n}\omega)}$. A comparison of Eqs. (6) and (7) with the numerically evaluated exact rate of Eq. (3) is shown in Ref. [28].

Since the nonadiabatic corrections raise the energy level, the tunnel exit shifts closer to the atomic core, which increases the ionization probability, displayed as a shrinking of the mentioned area. Furthermore, in the case of circular polarization, part of the energy of the tunneling electron is transferred into the transversal direction (see below), decreasing the longitudinal energy $\mathcal{E}_\parallel$ and, consequently, the energy level $\mathcal{E}(x)$, which yields a smaller tunneling probability compared to the linear polarization case; see Fig. 1.

We can also deduce from Eq. (6) the most probable momentum of the electron at the tunnel exit which corresponds to the minimum of $\mathrm{Im}\{S_L(t_e, t_s, \mathbf{p}) - I_p t_s\}$. In contrast to the quasistatic tunneling case ($\gamma \ll 1$), the tunneling probability $\Gamma(p_{\perp e})$ at an intermediate $\gamma \sim 1$ has a maximum at a nonzero value of the transverse momentum $p_{\perp e} = \epsilon\gamma\kappa/6$; see Fig. 2(c). An order of magnitude estimation confirms that the nonvanishing momentum at the tunnel exit is due to the nonvanishing transversal electric force of the rotating field of the elliptically polarized laser field $E_\perp(\tau_k) \sim \epsilon E_0 \gamma$. In fact, the transversal force induces the momentum change during tunneling $\Delta p_\perp \sim E_\perp(\tau_k)\tau_k \sim \epsilon\gamma\kappa$, with the Keldysh time $\tau_k \sim \gamma/\omega = \kappa/E_0$. For the most probable tunneling electron trajectory, this momentum change has to be compensated for by a transversal momentum in the opposite direction at the ionic core, yielding at the tunnel exit the electron transverse momentum in the direction of the transverse force. It is very similar to relativistic tunnel ionization, where the transversal Lorentz-force is due to the magnetic field component [27,29]. The momentum shift due to nonadiabatic effects is also visible in the asymptotic momentum distribution at the detector. In the static model the maximal final momentum is $p_f \sim \epsilon E_0/\omega$, whereas in the nonadiabatic regime the momentum shift during tunneling is added, yielding $p_f \sim \epsilon E_0/\omega + p_{\perp e}$; see Fig. 2(a).

While the simple case of a short-range atomic potential was suitable to describe the qualitative modification of the tunneling picture in the case of nonadiabatic ionization, the effect of the Coulomb field of the atomic core should be taken into account for quantitative predictions [30–33]. In the case of the Coulomb atomic potential $V_C(r) = -Z/r$, where Z is the charge of the ionized atom, the ionized wave packet in the remote future can be given via

$$\psi(\mathbf{p}) \sim \int_{-\infty}^{\infty} dt \int d^3\mathbf{r} E(t) \times \exp\left[-iS_{\mathrm{LC}}(\mathbf{r}, t) + \frac{Z}{\kappa}\ln x + iI_p t - \kappa r\right], \quad (8)$$

where the second term in the exponent arises from the SFA matrix element and further terms from the bound state wave function [28]. S_{LC} is the classical action in the laser and the Coulomb field and fulfills the Hamilton-Jacobi equation:

$$-\partial_t S_{\mathrm{LC}} = (\nabla S_{\mathrm{LC}})^2/2 + V_C(r) + \mathbf{r}\cdot\mathbf{E}(t). \quad (9)$$

The four-dimensional integral in Eq. (8) can be solved with the saddle point method that yields the saddle point conditions for the initial time and the coordinate of the ionizing electron [28]. From the latter the initial coordinate and the initial velocity are determined as a function of the initial time t_s, with complex values for the saddle time and the coordinate. The latter is used to calculate the electron trajectory (under the barrier and outside the barrier) by numerically solving Newton equations of motion in the Coulomb and laser fields and finding the final most probable momentum. To understand how the final momentum is modified, we analyze the modification of the electron parameters when appearing in the continuum. For the most probable trajectory, the electron leaves the barrier when the coordinate becomes real ($\mathrm{Im}\{x(t_e)\} = 0$) and the electron velocity along the tunneling direction is vanishing $\dot{x}(t_e) = 0$ [28]. These conditions define the coordinate of the tunnel exit, yielding the Coulomb-corrected exit $x(t_e)$ and the transversal exit momentum $\dot{y}(t_e)$; see Figs. 2(b) and 2(c).

The reduction of the exit coordinate compared to the zero-range potential case can be understood via the attractive longitudinal Coulomb force which decreases the tunneling distance. Transversally the Coulomb and the laser force have opposite signs and compensate for each other such that the required initial momentum to return to the real axis is smaller for the Coulomb potential than for the zero-range potential case. In total, the under-the-barrier trajectory is more focused along the main tunneling direction due to the Coulomb force of the atomic core. There is one property of the nonadiabatic under-the barrier motion in the case of a Coulomb potential which is qualitatively different from the case of a short-range atomic potential: in the most probable trajectory, the electron starts leaving the bound state before the peak of the laser field but exits the barrier after the maximum of the laser field [see Figs. 2(d) and 2(e)]. This induces a nonadiabatic time delay $t_e - t_0$, where t_0 corresponds to the peak of the laser field, which can be equivalently described by a longitudinal momentum at the tunnel exit. It vanishes in the limit $\gamma \ll 1$ (at $E \ll E_a$)—see Fig. 2(e)—and is of different origin than the tunneling time delay [34–36]. The nonadiabatic time delay is due to two factors: the ionization barrier is changing during the tunneling formation in the nonadiabatic case, and the bound state is not localized in the case of a Coulombic atomic potential [28].

Now we turn to the question of attoclock calibration. For this purpose one has to accurately take into account

Coulomb focusing during the electron propagation in the continuum after exiting the ionization barrier which affects the photoelectron emission angle. We use the calculated exit coordinate, the transverse momentum shift at the exit, and the exit time as starting conditions for the continuum motion. In Fig. 2(f) we show that with our simple model the experimental data on the asymptotic emission angle can be reproduced if nonadiabatic corrections and the Coulomb field for the under-the-barrier motion are accounted for. Note that the shift of the tunneling exit closer to the core in the nonadiabatic case increases the Coulomb focusing in the continuum, whereas the initial transverse momentum counteracts it. While in a short-range atomic potential these two effects compensate for each other, in the case of a Coulomb atomic potential the first contribution dominates. The impact of the nonadiabatic time delay on the photoelectron emission angle is even smaller [28].

In conclusion, an intuitive model for the intermediate regime of tunneling and multiphoton ionization has been developed. This way the photoelectron momentum distribution in the recent attoclock experiments is explained mostly by Coulomb focusing due to a displacement of the tunnel exit and without invoking the tunneling time delay.

M. K. acknowledges his fruitful discussions with Anton Wöllert, Enderalp Yakaboylu, and John Briggs. We also thank Robert Boge and Ursula Keller for providing the experimental data in Fig. 2(f).

*Corresponding author.
k.hatsagortsyan@mpi-k.de

[1] M. Protopapas, C. H. Keitel, and P. L. Knight, Rep. Prog. Phys. **60**, 389 (1997).
[2] W. Becker, F. Grasbon, R. Kopold, D. Milošević, G. G. Paulus, and H. Walther, Adv. At. Mol. Opt. Phys. **48**, 35 (2002).
[3] L. V. Keldysh, Zh. Eksp. Teor. Fiz. **47**, 1945 (1964).
[4] P. B. Corkum, Phys. Rev. Lett. **71**, 1994 (1993).
[5] M. Y. Ivanov, M. Spanner, and O. Smirnova, J. Mod. Opt. **52**, 165 (2005).
[6] R. Boge, C. Cirelli, A. S. Landsman, S. Heuser, A. Ludwig, J. Maurer, M. Weger, L. Gallmann, and U. Keller, Phys. Rev. Lett. **111**, 103003 (2013).
[7] F. H. M. Faisal, J. Phys. B **6**, L89 (1973).
[8] H. R. Reiss, Phys. Rev. A **22**, 1786 (1980).
[9] A. M. Perelomov and V. S. Popov, Zh. Eksp. Teor. Fiz. **50**, 1393 (1966).[Sov. Phys. JETP. **23**, 924 (1966)].
[10] A. M. Perelomov, V. S. Popov, and V. M. Terent'ev, Zh. Eksp. Teor. Fiz. **51**, 309 (1966).[Sov. Phys. JETP. **24**, 207 (1966)].
[11] A. M. Perelomov and V. S. Popov, Zh. Eksp. Teor. Fiz. **52**, 514 (1967).[Sov. Phys. JETP. **25**, 336 (1967)].
[12] V. S. Popov, V. P. Kuznetsov, and A. M. Perelomov, Zh. Eksp. Teor. Fiz. **53**, 331 (1967).[Sov. Phys. JETP. **26**, 222 (1968)].
[13] V. S. Popov, Phys. Usp. **47**, 855 (2004).
[14] G. L. Yudin and M. Y. Ivanov, Phys. Rev. A **64**, 013409 (2001).
[15] V. D. Mur, S. V. Popruzhenko, and V. S. Popov, Zh. Eksp. Teor. Fiz. **119**, 893 (2001).
[16] S. V. Popruzhenko, V. D. Mur, V. S. Popov, and D. Bauer, Phys. Rev. Lett. **101**, 193003 (2008).
[17] D. I. Bondar, Phys. Rev. A **78**, 015405 (2008).
[18] I. Barth and O. Smirnova, Phys. Rev. A **84**, 063415 (2011).
[19] A. N. Pfeiffer, C. Cirelli, M. Smolarski, D. Dimitrovski, M. Abu-samha, L. B. Madsen, and U. Keller, Nat. Phys. **8**, 76 (2012).
[20] P. Eckle, M. Smolarski, F. Schlup, J. Biegert, A. Staudte, M. Schöffler, H. G. Muller, R. Dörner, and U. Keller, Nat. Phys. **4**, 565 (2008).
[21] P. Eckle, A. N. Pfeiffer, C. Cirelli, A. Staudte, R. Dörner, H. G. Muller, M. Büttiker, and U. Keller, Science **322**, 1525 (2008).
[22] A. N. Pfeiffer, C. Cirelli, M. Smolarski, and U. Keller, Chem. Phys. **414**, 84 (2013).
[23] I. A. Ivanov and A. S. Kheifets, Phys. Rev. A **89**, 021402 (2014).
[24] L. Torlina and O. Smirnova, Phys. Rev. A **86**, 043408 (2012).
[25] J. Kaushal and O. Smirnova, Phys. Rev. A **88**, 013421 (2013).
[26] L. Torlina, F. Morales, J. Kaushal, H. Geert Muller, I. Ivanov, A. Kheifets, A. Zielinski, A. Scrinzi, M. Ivanov, and O. Smirnova, arXiv:1402.5620.
[27] E. Yakaboylu, M. Klaiber, H. Bauke, K. Z. Hatsagortsyan, and C. H. Keitel, Phys. Rev. A **88**, 063421 (2013).
[28] See Supplemental Material at http://link.aps.org/supplemental/10.1103/PhysRevLett.114.083001 for a detailed derivation of Eqs. (4)–(7).
[29] M. Klaiber, E. Yakaboylu, H. Bauke, K. Z. Hatsagortsyan, and C. H. Keitel, Phys. Rev. Lett. **110**, 153004 (2013).
[30] S. V. Popruzhenko, G. G. Paulus, and D. Bauer, Phys. Rev. A **77**, 053409 (2008).
[31] S. V. Popruzhenko and D. Bauer, J. Mod. Opt. **55**, 2573 (2008).
[32] T.-M. Yan and D. Bauer, Phys. Rev. A **86**, 053403 (2012).
[33] S. V. Popruzhenko, J. Exp. Theor. Phys. **118**, 580 (2014).
[34] E. P. Wigner, Phys. Rev. **98**, 145 (1955).
[35] D. Sokolovski, in *Time in Quantum Mechanics*, Lecture Notes in Physics Vol. 734, edited by J. G. Muga, R. Mayato, and I. L. Egusquiza (Springer, Berlin, 2008), p. 195.
[36] E. Yakaboylu, M. Klaiber, and K. Z. Hatsagortsyan, Phys. Rev. A **90**, 012116 (2014).